Scale effects in GFRPbar reinforced concrete beams

Received: 12 July 2022 | Revised: 18 October 2022 | Accepted: 26 January 2023

DOI: 10.1002/suco.202200676

ARTICLE

fib CEB-FIP WILEY

Scale effects in GFRP-bar reinforced concrete beams

Federico Accornero[1,2] | **Renato Cafarelli**[1] | **Alberto Carpinteri**[1,2] | **Antonio Nanni**[3]

[1]Department of Structural, Geotechnical and Building Engineering, Politecnico di Torino, Turin, Italy

[2]Department of Civil and Environmental Engineering, Shantou University, Shantou, People's Republic of China

[3]Civil and Architectural Engineering Department, University of Miami, Coral Gables, Florida, USA

Correspondence
Federico Accornero, Politecnico di Torino, Italy; Shantou University, China.
Email: federico.accornero@polito.it

Abstract

Glass fiber-reinforced polymer (GFRP)-reinforced concrete (RC) can be defined as a cementitious material in which the reinforcing secondary phase consists in corrosion-resistant GFRP rebars. For this next-generation structural material, experimental flexural tests highlight how the postcracking response is strongly affected by the amount of GFRP area together with the structural size-scale. In this work, the cohesive/overlapping crack model (COCM) is adopted to describe the transition between cracking and crushing failures occurring in GFRP-RC beams by increasing the beam depth, the reinforcement percentage, and/or the concrete compression strength. Within this nonlinear fracture mechanics model, the tensile and compression ultimate behaviors of the concrete matrix are modeled through two different process zones that advance independently one of another. Moreover, this model is able to investigate local mechanical instabilities occurring in the structural behavior of GFRP-RC beams: tensile snap back and snap-through, which are due to concrete cracking and reinforcement bridging action, and the compression snap-back generated by the unstable growth of the crushing zone. In this context, the application of the COCM highlights that the ductility, which is represented by the plastic rotation capacity of the GFRP-RC beam only when the reinforcement can slip, decreases as reinforcement percentage and/or beam depth increase. In this way, rational and quantitative definitions of hyperstrength and brittle compression crushing behaviors can be provided as a GFRP percentage depending on the beam depth.

KEYWORDS

cohesive/overlapping crack model, fracture mechanics, GFRP-RC, minimum reinforcement, size-scale effects

1 | INTRODUCTION

In 2016, a study performed by the National Association of Corrosion Engineers[1] estimated that the impact to the global world economy of the corrosion of steel bars used in reinforced concrete (RC) was around 2.5 trillion dollars (mainly due to emergency decommissioning of structures). It results the need for maintenance, retrofitting, or eventually rebuilding from the ground the infrastructure network. Due to this issue, starting from the end of the last century, the use of a new type of reinforcement, which substitutes corrosion-sensitive steel bars, has been taken into consideration. The solution is represented by glass fiber-reinforced polymer (GFRP) bars that, thanks to the properties of the polymer matrix, are completely corrosion free.[2–7]

Generally speaking, if we consider the stress–strain behavior of GFRP bars, no ductile behavior can be expected: after the peak stress, ranging from 450 to 1600 MPa, we acknowledge the brittle rupture of the reinforcement.[5–7]

On the other hand, GFRP bars can show a ductile postpeak behavior if we consider their bond-slip constitutive law.[8] In Figure 1, pull-out curves obtained for GFRP bars with three different types of coating are shown.[9] The difference between bar coatings is related to the difference in roughness of the bar surface. In the case of red curves, we have the bond-slip behavior of GFRP bars with a coating very similar to that of traditional steel bars: The surface ribs guarantee a perfect bond between bar and concrete matrix. As a consequence, the GFRP bar, after the initial elastic branch, presents a bond stress peak and then a brittle rupture. On the contrary, in the case of gray and blue curves, we acknowledge an elastic branch up to the peak and then a pseudo-plastic plateau that represents the slippage of the bar inside the concrete matrix instead of the plastic behavior of the material. In general, we can say that in the case of perfect bond between GFRP bar and concrete matrix, an elastic-perfectly brittle constitutive law is described. On the contrary, when the bond level between bar and concrete matrix is low, we can acknowledge a ductile behavior due to the bar pull-out from the concrete matrix.

GFRP-RC can be considered as a quite new structural material.[3,10–13] Therefore, only few international codes provide a framework of standards in order to design GFRP-RC. In particular, referring to the theoretical framework offered by AASHTO,[14] ACI,[15,16] and FIB,[17] current structural design is based on the GFRP bar constitutive law represented by the stress–strain relationship that shows brittle rupture after peak stress, without any possibility of plastic rotation capacity for the RC structural element. These codes identify the optimum structural condition in the so-called "balanced condition," or "maximum reinforcement condition," which is treated as the lower limit for a correct design (Figure 2). It is worth recalling that the maximum reinforcement condition gives the quantity of reinforcement beyond which brittle compression crushing in the concrete matrix is triggered. From a fracture mechanics point of view, considering that no plastic plateau can be envisaged in the stress–strain behavior of GFRP bars, current AASHTO, ACI, and FIB codes offer an unsafe approach that considers only structural brittleness instead of ductility, which, on the contrary, is a crucial characteristic for a correct structural design. In order to overcome these evident shortcomings, several parametric analyses are performed in the following by means of the cohesive/overlapping crack model (COCM).[18–22]

2 | THE COHESIVE/OVERLAPPING CRACK MODEL

The cohesive crack model[23,24] has been adopted as a powerful tool in the investigation of the ductile-to-brittle

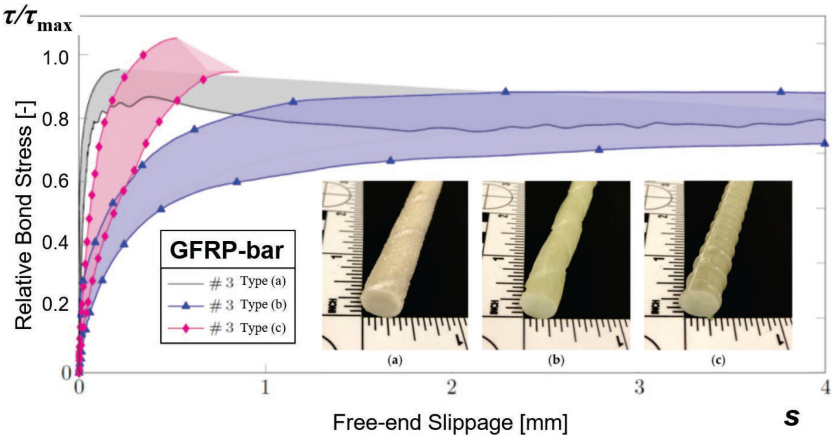

FIGURE 1 Bond-slip constitutive laws of glass fiber-reinforced polymer (GFRP) bars with different types of coating (from Emparanza et al.[9]): (a) Sand coating; (b) Helycal wraps; (c) Ribs.

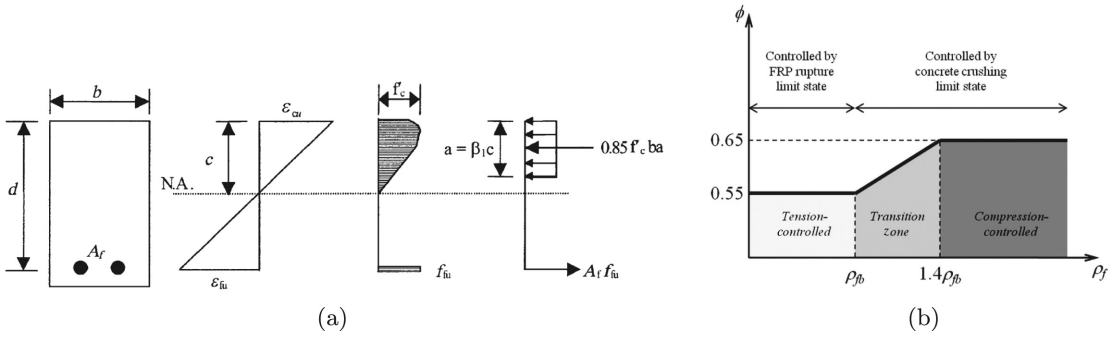

FIGURE 2 ACI 440.1-R15[15]: (a) Balanced condition; (b) Resistance factor versus reinforcement percentage.

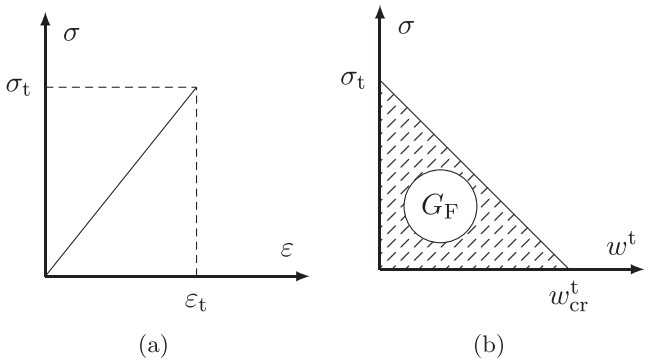

FIGURE 3 Cohesive Crack Model: (a) Linear elastic stress–strain law; (b) Postpeak σ–w_t cohesive relationship.

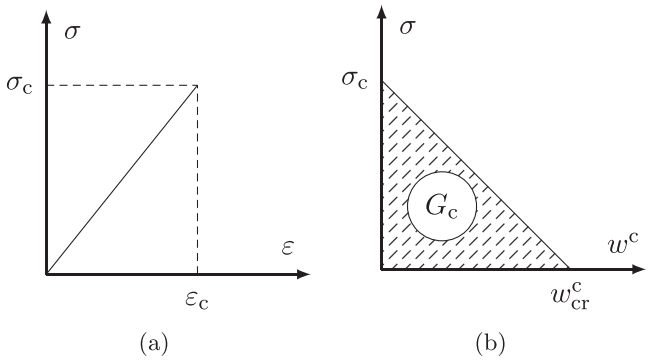

FIGURE 4 Overlapping Crack Model: (a) Linear elastic stress–strain law in compression; (b) Postpeak stress versus fictitious interpenetration relationship.

transition occurring in concrete elements as a function of beam depth, h, material tensile strength, σ_t, and fracture energy, G_F. The behavior of the undamaged material is represented by means of a linear elastic constitutive law, which is defined in the σ–ε diagram (Figure 3a). On the other hand, in the zone where strain-localization occurs, a constitutive law can be defined in the σ–w_t diagram (Figure 3b), being w_t the crack opening displacement. The area subtended by the σ–w_t curve represents the fracture energy, G_F, which is an actual material property independent of the beam depth, h.

On the other hand, the overlapping crack model[25] was introduced in order to simulate the compression damage of concrete occurring at the beam extrados. In close analogy to the cohesive crack model, the overlapping crack model assumes two constitutive laws for concrete in compression: the behavior of the undamaged material is modeled in the σ–ε diagram (Figure 4a), whereas a constitutive law defined in a σ–w_c diagram is used in the damaged zone (Figure 4b), w_c being an overlapping displacement discontinuity representing strain-localization in compression and possible extreme phenomena of ejection. The area subtended by the σ–w_c curve is the crushing energy, G_c, which presents the same physical dimensions as the fracture energy G_F.[25–28]

In the COCM,[28] the two above-mentioned constitutive laws are integrated in order to take into account the concrete nonlinear behavior both in tension and in compression. Due to its characteristics, this fracture mechanics model is particularly suitable in the investigation of over-reinforced concrete beams, since matrix compression crushing represents the dominant phenomenon in the postcracking regime. In the framework of COCM, the beam cross section is divided into n nodes (Figure 5), for which the following linear elastic equation can be written:

$$\{w\} = [K_F]\{F\} + \{K_M\}M \tag{1}$$

where $\{w\}$ is the vector of the opening/overlapping displacements; $[K_F]$ is the matrix containing the nodal displacements generated by unit nodal forces; $\{F\}$ is the vector of nodal forces; $\{K_M\}$ is the vector containing the nodal displacements generated by a unit bending moment; M is the applied bending moment. The unknowns involved in Equation (1) are $(2n + 1)$ and have both static and kinematic nature. In the general case of Figure 5, it is possible to consider the following conditions (Figures 3b and 4b):

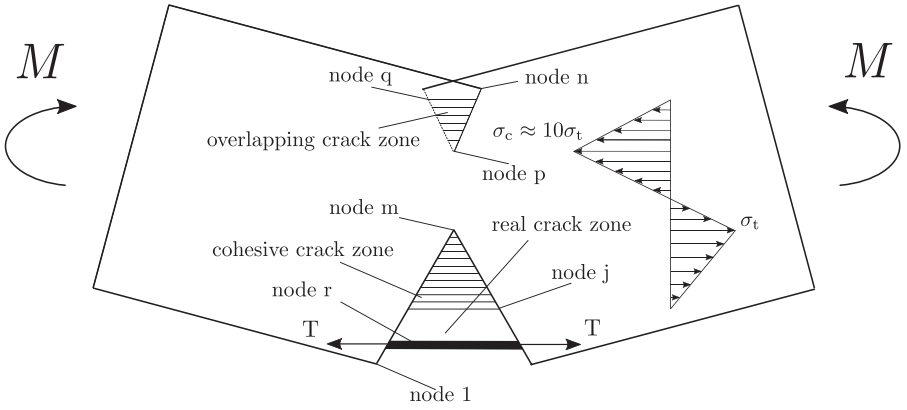

FIGURE 5 Cohesive/Overlapping Crack Model.

$$F_i = 0 \quad \text{for} \quad i = 1,...,(j-1), i \neq r \tag{2a}$$

$$F_i = F_t\left(1 - \frac{w_i}{w_{cr}^t}\right) \quad \text{for} \quad i = j,...,(m-1) \tag{2b}$$

$$w_i = 0 \quad \text{for} \quad i = m,...,p \tag{2c}$$

$$F_i = F_c\left(1 - \frac{w_i}{w_{cr}^c}\right) \quad \text{for} \quad i = (p+1),...,q \tag{2d}$$

$$F_i = 0 \quad \text{for} \quad i = (1+q),...,n \tag{2e}$$

$$F_i = f(w_i) \quad \text{for} \quad i = r \tag{2f}$$

where j is the real cohesive crack tip; m is the fictitious cohesive crack tip; p is the fictitious overlapping zone tip; q is the real overlapping zone tip. Thus, the value of M is assumed as the minimum load that generates the ultimate tensile force, F_t, or the ultimate compressive force, F_c, in node m or p, respectively.

3 | PARAMETRIC ANALYSIS

As a first parametric analysis, a three-point bending test of a GFRP-RC beam in the case of perfect bond between GFRP bar and concrete matrix is considered. The beam has variable depth, h, and variable reinforcement percentage, whereas its span, ℓ, is fixed as four times the beam depth. The tensile strength of the concrete matrix, σ_t, is equal to 4 MPa, its compression strength, σ_c, is equal to 40 MPa, the concrete fracture energy, G_F, is equal to 0.08 N/mm, whereas the crushing energy, G_c, is equal to 30 N/mm. The GFRP bar, which is considered linear-elastic up to its rupture, has a tensile strength equal to 600 MPa. The bar rupture is triggered by a crack opening, w_r, equal to 3.1 mm, which is calculated following the procedure reported in Accornero et al.[18] and Ruiz.[24] In Figure 6, the moment versus rotation curves of the GFRP-RC beams are reported by considering four different reinforcement percentages: ρ = 0.2%, 0.4%, 0.6%, and 0.8%. For ρ = 0.2%, different structural behaviors are shown by varying the beam depth, from curve A (h = 0.2 m), to curve F (h = 2 m). All the hardening branches represent the different postcracking behaviors of the GFRP-RC beams, which are characterized by the GFRP bar rupture, thus showing a negligible rotation capacity. By increasing the reinforcement percentage, we move from a brittle behavior due to the reinforcement rupture in tension to a similar brittle behavior due to the matrix concrete crushing in compression. For ρ = 0.8%, we have final softening due to compression crushing for small beam depth (h = 0.2; 0.4 m), whereas for $h \geq 0.6$ m catastrophic failures due to brittle compression crushing of the concrete matrix are revealed (snap-back instability). Generally speaking, by varying GFRP reinforcement percentage and beam scale, we move very unsafely from a brittle failure in tension to a brittle failure in compression (snap-back) without any ductile behavior.

As a second GFRP-RC parametric analysis, we consider a GFRP reinforcement that can slip inside the concrete matrix (Figure 7). The mechanical characteristics of the concrete matrix are the same as in the previous analysis, whereas in this case, the GFRP bar presents an average slippage strength equal to 1 MPa (bond-slip constitutive law). For the moment versus rotation curves characterized by ρ = 0.2%, the beam with h = 0.2 m shows a safe rotation capacity, which is described by a wide pseudo-plastic plateau. By increasing the beam depth, from curve B to curve E, we can acknowledge a progressive decrease in plastic rotation capacity: for h = 1 m, we have brittle concrete crushing prior to GFRP bar slippage. We can say that, whereas for traditional steel bar RC the maximum reinforcement condition describes the equilibrium point between concrete compression crushing and steel

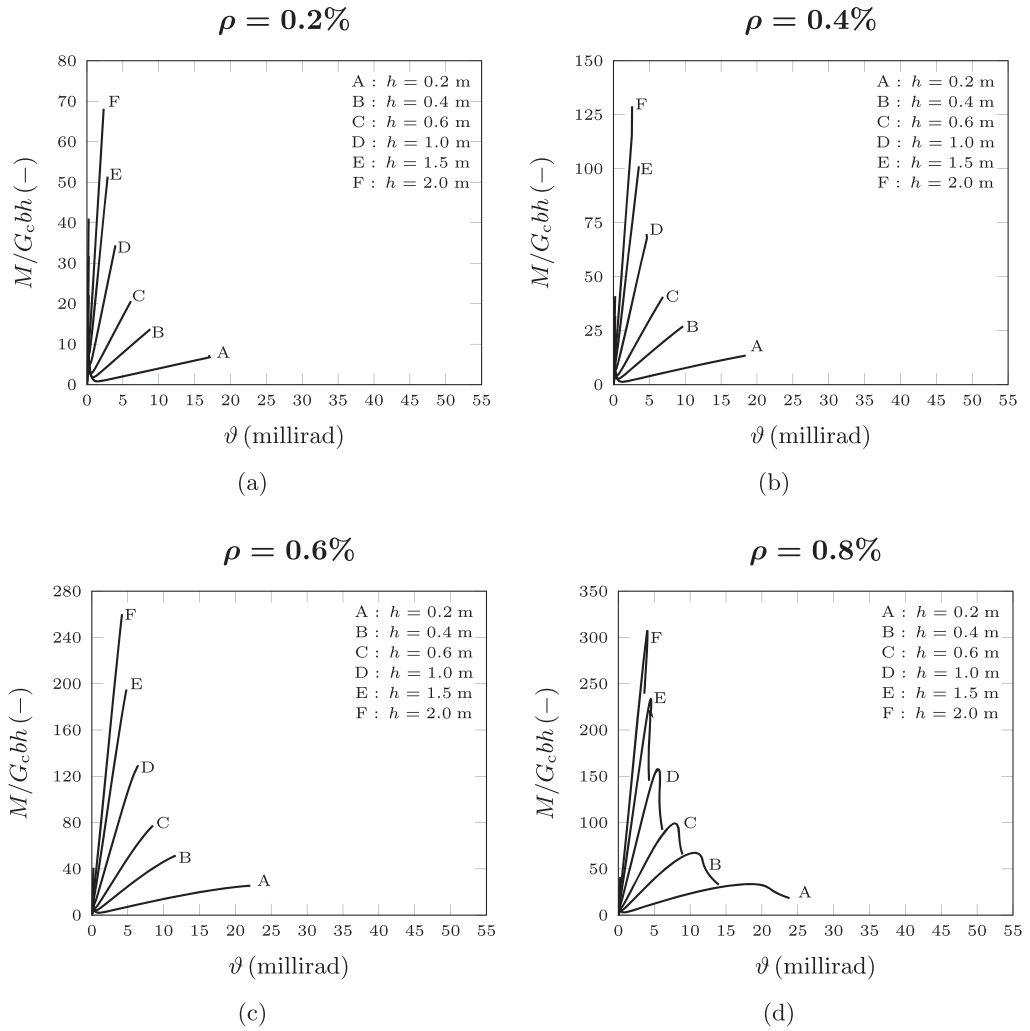

FIGURE 6 GFRP-RC parametric analysis considering a perfect bond between GFRP bar and concrete matrix (brittle behavior).

yielding, in the case of GFRP-RC this condition is balanced between concrete compression crushing and GFRP bar slippage. Moreover, by increasing the reinforcement percentage, we see a decrease in plastic rotation capacity also in the intermediate scales: for $\rho = 0.4\%$, the balanced condition is represented by $h = 0.8$ m, whereas in the case of $\rho = 0.8\%$, we acknowledge a balanced condition approaching to $h = 0.6$ m.

Then, focusing on the curves with $\rho = 0.2\%$, from $h = 0.2$ to 0.8 m, a hyperstrength behavior can be detected. As a matter of fact, the initial cracking moment is not recovered by the ultimate bending moment of the GFRP-RC beam. In particular, if the loading process is controlled by the load and not by the displacement, a sudden rupture of the structural element can be expected. Moreover, by increasing the beam depth, h, the gap between cracking moment and ultimate moment decreases, then approaching the minimum reinforcement condition.

4 | NUMERICAL VERSUS EXPERIMENTAL COMPARISON

In the following, a numerical versus experimental comparison is proposed to investigate size-scale effects on the structural behavior of GFRP-RC beams. Three different sizes, h, and two different reinforcement percentages, ρ, are considered (see Table 1). Tensile strength, σ_t, as well as fracture energy, G_F, of the concrete matrix are estimated according to Model Code 2010.[29] On the other hand, the crushing energy, G_c, is calculated by means of the formula proposed by Suzuki et al.[31] All the beams are tested up to failure following the loading scheme reported in Figure 8.

In Figure 9, the numerical (thick curve) versus experimental (thin curve) comparison is reported. Beam B1 shows a postcracking behavior characterized by a strong interaction between shearing and flexural failures, whereas for beams B2 and B3 COCM is able to

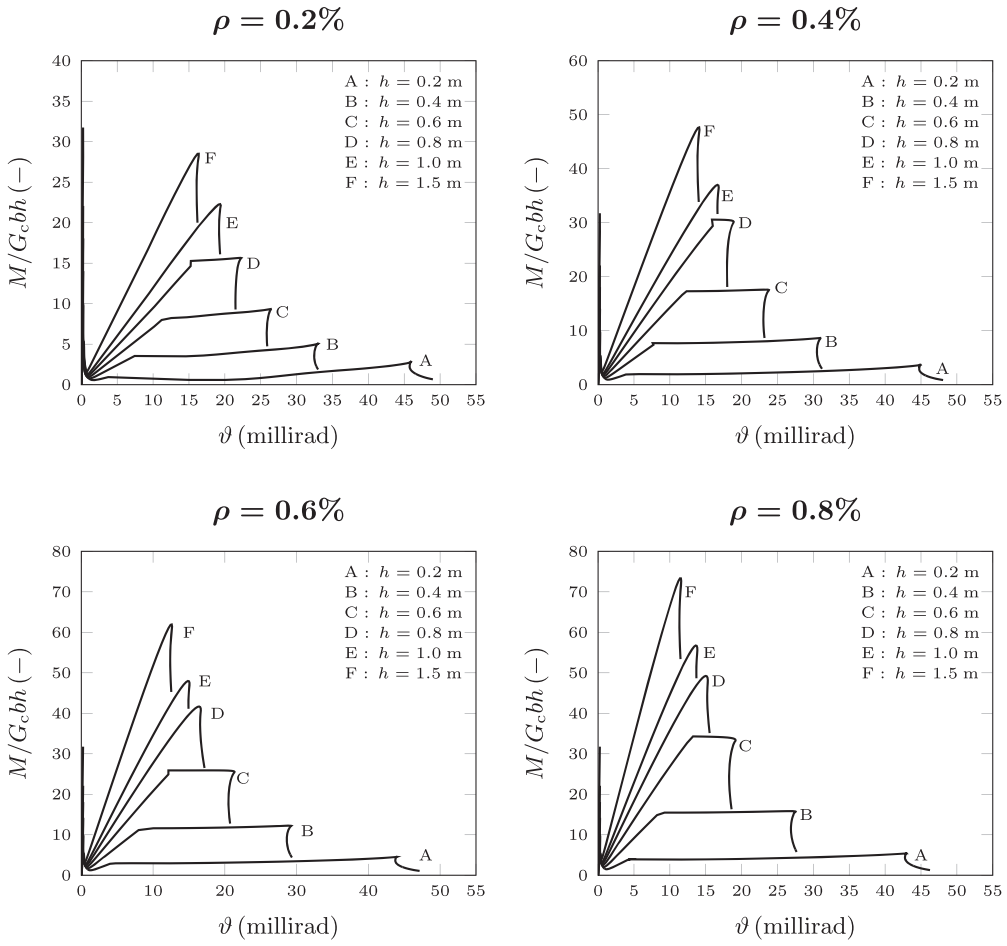

FIGURE 7 GFRP-RC parametric analysis considering a GFRP bar bond-slip constitutive law (ductile behavior).

TABLE 1 Testing specimens.

Beams No.	h (mm)	b (mm)	ℓ (m)	a (m)	σ_r (MPa)	ρ (%)	σ_c (MPa)	σ_t (MPa)	G_F (N/mm)	G_c (N/mm)
B1	102	102	0.61	0	700	0.69	31.0	3.0	0.141	30
B2	204	102	1.22	0.41	700	0.69	31.0	3.0	0.141	30
B3	300	180	2.8	1.2	700	0.79	35.0	3.2	0.144	30

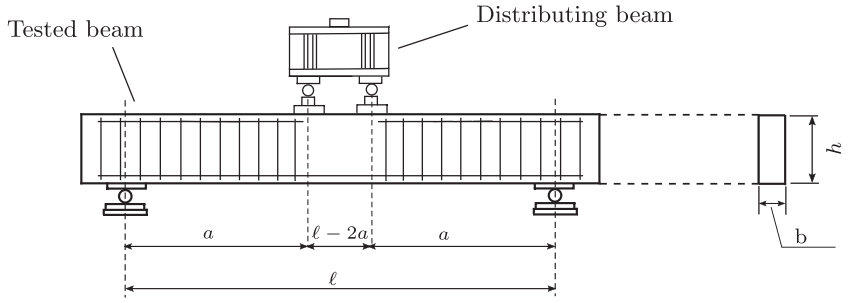

FIGURE 8 Testing set-up.

thoroughly predict their nonlinear behavior: after an initial snap-back triggered by concrete cracking, an ascending branch due to the activation of the GFRP internal reinforcement is acknowledged. This stable behavior is kept until the peak load, P_{max}, is reached. Beyond P_{max}, the strain-localization of concrete in compression makes the global structural behavior unstable and a catastrophic snap-back due to concrete compression crushing is revealed. Basically, as predicted above in the parametric analysis, by varying GFRP reinforcement percentage and

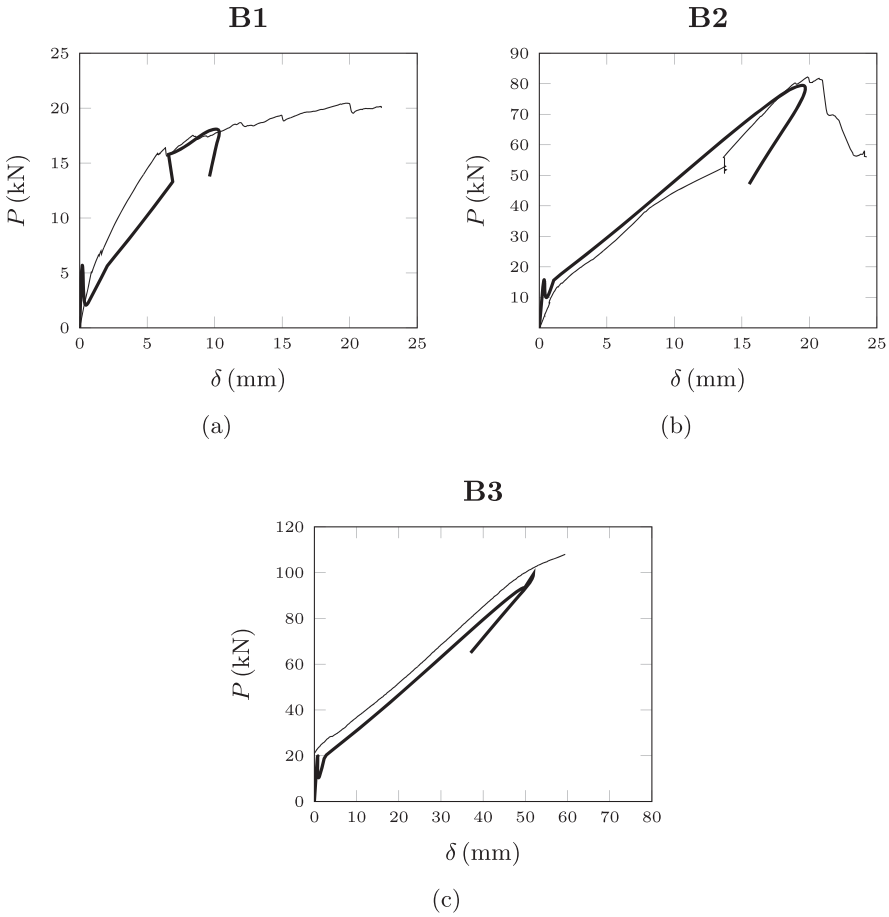

FIGURE 9 Numerical (thick) versus experimental (thin) curves: (a) $h = 102$ mm, (b) $h = 204$ mm, (c) $h = 300$ mm (from Toutanji and Saafi[30]).

beam scale, we move very unsafely from a brittle failure in tension to a brittle failure in compression (snap-back) without any evidence of plastic rotation capacity.

5 | DIMENSIONAL ANALYSIS AND MINIMUM REINFORCEMENT CONDITION

In order to define in a comprehensive way the size-scale effects previously highlighted, a dimensional analysis approach[32] can be considered. The flexural behavior of a GFRP-RC beam can be represented as:

$$M = F\left(\sigma_t, G_F, \sigma_c, G_c, E, \sigma_p, \rho, h; b/h, \ell/h; \vartheta\right) \tag{3}$$

The variables included in function F are: the tensile strength of the concrete matrix, σ_t, the matrix fracture energy, G_F, the matrix compression strength, σ_c, the matrix crushing energy, G_c, the Young's modulus of concrete, E, the GFRP bar equivalent strength (slippage), σ_p, the reinforcement percentage, ρ, and the beam scale, h, among others.

If we focus our attention to the minimum reinforcement percentage, all the variables in the previous equation referring to concrete compression behavior can be neglected:

$$M = F\left(\sigma_t, G_F, E, \sigma_p, \rho, h; b/h, \ell/h; \vartheta\right) \tag{4}$$

Applying Buckingham's Theorem[32] and assuming as independent variables h and G_F, we have:

$$\frac{M}{\sqrt{G_F E} h^{2.5}} = \Pi\left(\frac{\sqrt{G_F E}}{\sigma_t h^{0.5}}, \rho\frac{\sigma_p h^{0.5}}{\sqrt{G_F E}}, \vartheta\frac{\sqrt{G_F E}}{E h^{0.5}}\right) \tag{5}$$

Normalizing function F, we obtain the Buckingham's function Π, in which the matrix brittleness number, $s_t = (G_F E)^{0.5}/\sigma_t h^{0.5}$, and the reinforcement brittleness number, $N_P = \rho\sigma_P h^{0.5}/(G_F E)^{0.5}$, are obtained.

Therefore, a numerical study can be performed in order to determine the GFRP-RC minimum reinforcement percentage, ρ_{min}, based on a s_t versus N_{PC} diagram. In Figure 10, N_{PC} is proportional to the minimum reinforcement percentage, ρ_{min}, able to guarantee a stable

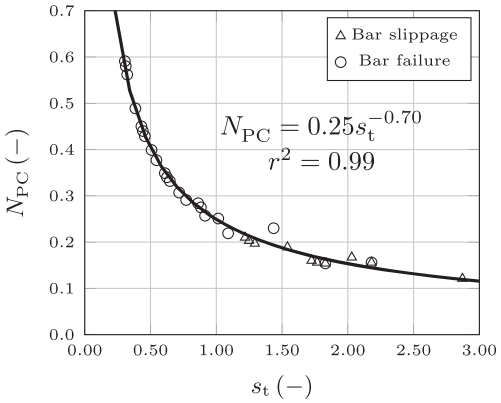

FIGURE 10 GFRP-RC minimum reinforcement condition.

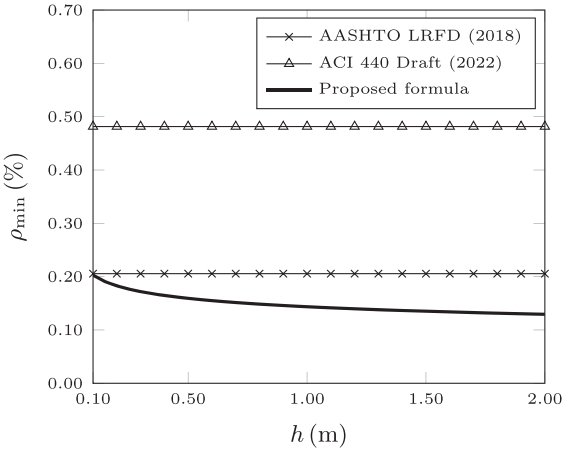

FIGURE 11 Minimum GFRP reinforcement percentage: Comparison between AASHTO[14] provisions, ACI draft,[16] and the proposed formula.

postcracking response of the GFRP-RC beams. On the other hand, by making ρ_{min} explicit, we have:

$$\rho_{min} = 0.25 \frac{\sigma_t^{0.7} \left(\sqrt{G_F E}\right)^{0.3}}{\sigma_p h^{0.15}} \tag{6}$$

where a scale effect on GFRP-RC minimum reinforcement percentage is found to be $h^{-0.15}$. It is worth noting that, since the bond between the GFRP bar and the concrete matrix is highly dependent on the roughness of the bar surface,[6,33–35] both bar slippage and bar rupture conditions are considered in Figure 10.

Finally, a comparison is made between the minimum GFRP reinforcement percentages provided by AASHTO,[14] ACI,[16] and that obtained by the above-mentioned formula. In Figure 11, only AASHTO minimum reinforcement percentage turns to be equal to the one proposed through the present fracture mechanics approach for the scale $h = 0.1$ m, whereas for larger scales the constant reinforcement percentage proposed by AASHTO seems to be rather ineffective.

6 | CONCLUSIONS

In this paper, the COCM is adopted to investigate scale effects on the structural behavior of GFRP-RC beams. This fracture mechanics model highlights how, in the case of perfect bond between GFRP internal reinforcement and concrete matrix, a brittle failure characterized by the reinforcement rupture or the matrix compression crushing is obtained. On the other hand, in the case of weaker rebar–matrix bond, a global ductile behavior characterized by the GFRP bar pull-out is acknowledged. The parametric studies carried out by means of the COCM describe a ductile-to-brittle transition that is triggered by varying the rebar slippage strength, the reinforcement percentage, ρ, and/or the beam size, h. In this framework, a rational and accurate minimum reinforcement percentage, ρ_{min}, proportional to $h^{-0.15}$, can be provided to make current Standards safer and more effective.

NOTATIONS

ϑ	beam rotation
ℓ	beam span
$[K_F]$	matrix of nodal displacements generated by unit forces
$\{F\}$	vector of nodal forces
$\{K_M\}$	vector of nodal displacements generated by unit bending moment
$\{w\}$	vector of nodal displacements
a	beam shear span
b	beam thickness
G_c	crushing energy
G_F	fracture energy
h	beam depth
M	bending moment
n	numbers of nodes used to discretized the beam section
N_P	reinforcement brittleness number
P	load
P_{max}	maximum load
s_t	matrix brittleness number
w^c	fictitious interpenetration
$w^c{}_{cr}$	critical value of fictitious interpenetration
w_r	crack opening generating reinforcement failure
w^t	crack opening
$w^t{}_{cr}$	critical value of crack opening
δ	deflection
ε_c	ultimate compressive strain of concrete
ε_t	ultimate tensile strain of concrete

ρ reinforcement percentage
ρ_{min} minimum reinforcement percentage
σ_c compression strength of concrete
σ_p reinforcement equivalent strength
σ_r reinforcement ultimate strength
σ_t tensile strength of concrete

DATA AVAILABILITY STATEMENT

The data that support the findings of this study are available on request from the corresponding author. The data are not publicly available due to privacy or ethical restrictions.

ORCID

Federico Accornero https://orcid.org/0000-0002-9638-8411
Renato Cafarelli https://orcid.org/0000-0003-2076-1053

REFERENCES

1. NACE. International measures of prevention, application, and economics of corrosion technologies (IMPACT) study. Houston, TX: NACE International; 2016.
2. De Luca A, Matta F, Nanni A. Behavior of full-scale glass fiber-reinforced polymer reinforced concrete columns under axial load. ACI Struct J. 2010;107:589–96.
3. Guérin M, Mohamed HM, Benmokrane B, Shield CK, Nanni A. Effect of glass fiber-reinforced polymer reinforcement ratio on axial-flexural strength of reinforced concrete columns. ACI Struct J. 2018;115:1049–61.
4. Morales CN, Claure G, Nanni A. Flexural and durability performance of seawater-mixed glass fiber-reinforced polymer-reinforced concrete slabs. ACI Struct J. 2022;119:105–18.
5. Nanni A. Flexural behavior and design of RC members using FRP reinforcement. ASCE J Struct Eng. 1993;119:3344–59.
6. Nanni A, De Luca A, Jawahei Zadeh H. Reinforced concrete with FRP bars. Boca Raton: CRC Press; 2014.
7. Alsayed SH, Al-Salloum YA, Almussallam TH. Performance of glass fiber reinforced plastic bars as reinforcing material for concrete structures. Composites Part B. 2000;31:555–67.
8. Pilakoutas K. Composites in concrete construction. In: Gdoutos A, Pilakoutas K, Rodopoulos C, editors. Failure analysis of industrial composites materials. McGraw-Hill; 2000. p. 449–97.
9. Ruiz Emparanza A, De Caso y Basalo F, Kampmann R, Adarraga Usabiaga I. Evaluation of the bond-to-concrete properties of GFRP rebars in marine environments. Infrastructures. 2018;3:44.
10. Benzecry V, Ruiz Emparanza A, De Casoy Basalo F, Nanni A. Bond coefficient, k_b, of GFRP bars. Construct Build Mater. 2021;292:123380.
11. Gooranorimi O, Suaris W, Nanni A. A model for the bond-slip of a GFRP bar in concrete. Eng Struct. 2017;146:34–42.
12. Reichenbach S, Preinstofer P, Hammerl M, Kromoser B. A review on embedded fibre-reinforced polymer reinforcement in structural concrete in Europe. Construct Build Mater. 2021;307:124946.
13. Rossini M, Saqan E, Nanni A. Prediction of the creep rupture strength of GFRP bars. Construct Build Mater. 2019;227:116620.
14. AASHTO. LRFD bridge design guide specifications for GFRP-reinforced concrete. Washington DC: AASHTO; 2018.
15. ACI. Guide for the design and construction of structural concrete reinforced with fiber-reinforced polymer (FRP) bars. Farmington Hills: ACI; 2015.
16. ACI. Guide for the design and construction of structural concrete reinforced with fiber-reinforced polymer (FRP) bars. ACI, Farmington Hills: Farmington Hills; 2022.
17. fib (Fédération Internationale du Béton) Bulletin 40. FRP reinforcement in RC structures. Lausanne (Switzerland): Fédération internationale du Béton (FIB); 2007.
18. Accornero F, Cafarelli R, Carpinteri A. Cracking and crushing in prestressed concrete beams. ACI Struct J. 2021;118:101–9.
19. Accornero F, Cafarelli R, Carpinteri A. The cohesive/overlapping crack model for plain and reinforced concrete beams: scale effects on cracking and crushing failures. Mag Concr Res. 2022;74:433–50.
20. Carpinteri, A., Accornero, F., Cafarelli, R., Ductile-to-brittle transition in RC and PC beams: scale effects on minimum and maximum reinforcements. In: Zhao B, Lu X, editors. Proceedings of the FIB symposium 2020, Shanghai, China; 2020, p. 1115–1122.
21. Carpinteri A, Accornero F, Cafarelli R. Scale-dependent maximum reinforcement percentage in RC beams. fib Struct Concr. 2021;22:2155–66.
22. Carpinteri A, Accornero F, Cafarelli R. Scale effects in prestressed concrete structures: maximum reinforcement percentage to avoid brittle crushing. Eng Struct. 2022;255:113911.
23. Carpinteri A. Cusp catastrophe interpretation of fracture instability. J Mech Phys Solids. 1989;37:567–82.
24. Ruiz G. Propagation of a cohesive crack crossing a reinforcement layer. Int J Fract. 2001;111:265–82.
25. Carpinteri A, Corrado M, Mancini G, Paggi M. The overlapping crack model for uniaxial and eccentric concrete compression tests. Mag Concr Res. 2009;61:745–57.
26. van Mier JGM, Shah SP, Arnaud M, Balayssac JP, Bascoul A, Choi S, et al. "Strain-softening of concrete in uniaxial compression", report of the round Robin test carried out by RILEM TC 148-SCC. Mater Struct. 1997;30:195–209.
27. Jansen DC, Shah SP. Effect of length on compressive strain softening of concrete. J Eng Mech. 1997;123:25–35.
28. Carpinteri A, Corrado M, Mancini G, Paggi M. Size-scale effects on plastic rotational capacity of reinforced concrete beams. ACI Struct J. 2009;106(2009):887–96.
29. fib (Fédération Internationale du Béton). Model Code for Concrete Structures 2010. New York, USA: John Wiley & Sons; 2013.
30. Toutanji HA, Saafi M. Flexural behaviour of concrete beams reinforced with glass fiber-reinforced polymer (GFRP) bars. ACI Struct J. 2000;97:712–9.
31. Suzuki M, Akiyama M, Matsuzaki H, Dang TH. Concentric loading test of RC columns with normal and high-strength materials and averaged stress-strain model for confined concrete considering compressive fracture energy. In: Proceedings of the second international fib congress, Doppiavoce, Naples, Italy; 2006.
32. Carpinteri A, Accornero F. Dimensional analysis of critical phenomena: self-weight failure, turbulence, resonance, fracture. Phys Mesomech. 2021;24:459–63.
33. Malvar LJ. Tensile and bond properties of GFRP reinforcing bars. ACI Struct J. 1995;92:276–85.

34. Cosenza E, Manfredi G, Realfonso R. Behaviour and modeling of bond of FRP rebars to concrete. ASCE J Compos Construct. 1997;1:40–51.
35. Pecce M, Manfredi G, Realfonzo G, Cosenza E. Experimental and analytical evaluation of bond properties of GFRP bars. ASCE J Mater Civ Eng. 2001;13:282–90.

AUTHOR BIOGRAPHIES

Federico Accornero
DISEG, Politecnico di Torino, Turin, Italy; College of Engineering, Shantou University, Shantou, China
Email: federico.accornero@polito.it

Renato Cafarelli
DISEG, Politecnico di Torino, Turin, Italy
Email: renato.cafarelli@polito.it

Alberto Carpinteri
DISEG, Politecnico di Torino, Turin, Italy; Department of Civil and Environmental Engineering, Shantou University, Shantou, China
Email: alberto.carpinteri@polito.it

Antonio Nanni
CAE, University of Miami, Coral Gables, Florida, USA
Email: ananni@miami.edu

How to cite this article: Accornero F, Cafarelli R, Carpinteri A, Nanni A. Scale effects in GFRP-bar reinforced concrete beams. Structural Concrete. 2023;24(2):2817–26. https://doi.org/10.1002/suco.202200676